International Journal of Pharmaceutics 678 (2025) 125729

Contents lists available at ScienceDirect

International Journal of Pharmaceutics

journal homepage: www.elsevier.com/locate/ijpharm

Targeted delivery of sorafenib via biotin decorated polyaminoaspartamide-based nanoparticles for the hepatocarcinoma treatment

Giulia Di Benedetto [a,1], Paola Varvarà [b,1], Salvatore Emanuele Drago [b], Anna Flavia Cantone [a], Nicolò Mauro [b], Gabriella Gaudio [a], Chiara Burgaletto [a], Carlo Maria Bellanca [a], Giuseppe Broggi [c], Rosario Caltabiano [c], Giovanna Pitarresi [b,*], Giuseppina Cantarella [a,**], Gaetano Giammona [b,2], Renato Bernardini [a,2]

[a] *Department of Biomedical and Biotechnological Sciences, Section of Pharmacology, University of Catania, Via Santa Sofia 97, 95123 Catania, Italy*

[b] *Laboratory of Biocompatible Polymers, Department of Biological, Chemical and Pharmaceutical Sciences and Technologies (STEBICEF), University of Palermo, Via Archirafi 32, 90123 Palermo, Italy*

[c] *Department of Medical, Surgical Sciences and Advanced Technologies "G.F. Ingrassia", Anatomic Pathology, University of Catania, Via Santa Sofia 87, 95123 Catania, Italy*

ARTICLE INFO

Keywords:
Polyaspartamide
Biotin
Sorafenib
Nanocarriers
Targeted delivery
Hepatocellular carcinoma

ABSTRACT

Hepatocellular carcinoma (HCC), the most common primary liver cancer, faces treatment challenges due to drug resistance and poor bioavailability, with sorafenib, a key therapy, characterized by rapid clearance and significant side effects. This paper describes the development of amphiphilic graft copolymers for efficient loading and delivery of sorafenib through controlled Atom Transfer Radical Polymerization (ATRP). The amphiphilic graft copolymer PHEA-g-IB-(pButMA)-g-PEG-Bt was synthesized to enhance tumor specificity via biotin-mediated targeting. The synthesis involved a three-step process, with successful functionalization confirmed through NMR and Size Exclusion Chromatography (SEC) analyses. Sorafenib-loaded nanoparticles, prepared via dialysis-based nanoprecipitation, exhibited a mean size of ~ 300 nm, suitable for oral and parenteral administration, while drug release studies confirmed a sustained release profile, minimizing premature systemic loss and reducing the need for frequent administration. Evaluation of cytocompatibility and anticancer efficacy tested in vitro on HepG2 and HuH-7 cell lines revealed that biotinylated sorafenib-loaded nanoparticles had the highest ability to reduce cell viability. The enhanced anticancer effect of biotinylated NPs was validated in vivo using a murine tumor xenograft model, as evidenced by reduced tumor growth, lower Ki-67 proliferation index, and diminished CD31-positive vasculature. Protein expression analysis demonstrated that PBB-Bt@SOR elicited the strongest activation of p-p38 MAPK and caspase-8-mediated apoptosis, while enhancing the expression of the pro-survival AKT pathway. Overall, the study confirms that biotinylated sorafenib-loaded nanoparticles improve tumor suppression in HCC models, demonstrating their effectiveness in targeted drug delivery. These findings suggest biotin decorated polyamino aspartamide-based nanoparticles as a promising strategy to optimize chemotherapy regimens, minimizing systemic toxicity in HCC treatment.

1. Introduction

Hepatocellular carcinoma (HCC), a primary liver cancer originating from hepatocytes (Bruix et al., 2019; Hu et al., 2023; Llovet et al., 2021, 2022), is associated with high incidence and mortality rates worldwide (Jemal et al., 2011). HCC often occur in individuals with chronic liver diseases, and conditions like hemochromatosis and alpha-1 antitrypsin deficiency significantly elevate the risk of developing HCC. HCC

---

* Corresponding author at: Via Archirafi 32, 90123 Palermo, Italy.

** Corresponding author at: Via Santa Sofia 97, 95123 Catania, Italy.

E-mail addresses: giovanna.pitarresi@unipa.it (G. Pitarresi), gcantare@unict.it (G. Cantarella).

[1] These authors share first authorship.

[2] These authors share senior authorship.

https://doi.org/10.1016/j.ijpharm.2025.125729
Received 7 April 2025; Received in revised form 12 May 2025; Accepted 13 May 2025

represent a highly vascularized tumor, with angiogenesis contributing to its rapid growth, invasion, and metastasis. Conventional therapeutic options have limitations in effectively managing HCC (Daher et al., 2018; Finn, 2013; Jemal et al., 2011), particularly in advanced stages neoplasms where surgery is often an unfeasible approach, and systemic chemotherapy efficacy is hindered by limited drug distribution, off-target toxicity, and the occurrence of drug resistance phenomena. In such scenario, innovative therapeutic approaches are essential for tackling the obstacles presented by HCC chemotherapy and improve the treatment outcomes. Nanomedicine, a branch of health sciences that employs nanotechnology to develop new therapeutic solutions, has gained significant interest in the field of HCC treatment (Fu et al., 2017; Hu et al., 2023; Landesman-Milo and Peer, 2016; Liu et al., 2015; Mauro et al., 2022; Wang et al., 2022; Yu et al., 2024), as these nanosystems can be designed to overcome the limitations of traditional approaches, therapeutic approaches, by providing targeted and controlled release of therapeutic agents, improve their stability and solubility, and minimize side effects, ultimately enhancing the therapeutic index (Böttger et al., 2020; Metkar et al., 2023; Scarabel et al., 2017). This approach is particularly relevant for the anticancer drugs sorafenib, the first drug currently approved by the US Food and Drug Administration (FDA) for first-line treatment of advanced HCC (Kane et al., 2009). Despite its antitumor efficacy, its use is associated with severe systemic side effects which significantly affect patients' quality of life (Abdel-Rahman and Lamarca, 2017).

Additionally, via the functionalization of nanocarriers surface with ligands, such as biotin, that specifically bind to receptors overexpressed in tumor cells (Giammona et al., 2022; Hu et al., 2015; Landesman-Milo and Peer, 2016; Singh et al., 2023), drug delivery can achieve greater specificity (Böttger et al., 2020).

Biotin receptors are overexpressed in HCC cells (Chen et al., 2019), making biotin-mediated targeting an attractive approach to enhance the selectivity of hepatocarcinoma treatment.

In such context, the present study aims to develop biotin-conjugated polymeric nanoparticles for the targeted delivery of sorafenib, known for its efficacy in HCC treatment, by virtue of overexpression of biotin receptor in HCC cells (Chen et al., 2019; Wang et al., 2025), enhancing the selectivity of hepatocarcinoma treatment. To achieve this, an amphiphilic copolymer was synthesized starting from α,β-poly(N-2-hydroxyethyl)-D,L-aspartamide (PHEA), a biocompatible water-soluble amino acid-based polymer, via Atom Transfer Radical Polymerization (ATRP) of butyl methacrylate (ButMA) to obtain the derivative PHEA-g-IB-pButMA, suitable for the preparation of nanoparticles (Cervello et al., 2017). Biotin residues were then introduced through functionalization with polyethylene glycol (PEG) as a spacer, enhancing surface biotin exposure while providing stealth properties to the nanosystems.

The efficacy of the nanoparticles as drug delivery systems was evaluated through both in vitro and in vivo studies. Cytocompatibility and anticancer efficacy of sorafenib-loaded biotin-conjugated polymeric nanoparticles were assessed in vitro using human HCC cell lines. Subsequently, these nanoparticles were administered orally in a xenograft model established by inoculating human HCC cells in male nude athymic mice. The effect of the newly developed drug delivery systems on tumour progression was then examined in terms of tumor suppression efficacy and therapeutic performance compared to conventional sorafenib delivery. This approach is particularly relevant given that sorafenib remains a first-line systemic treatment in advanced HCC (Hu et al., 2023; Llovet et al., 2021), and that biotin-mediated targeting strategies may help enhance selectivity and reduce systemic toxicity (Wang et al., 2025).

2. Materials and methods

2.1. Materials

α, β-poly(N-2-hydroxyethyl)-D,L-aspartamide (PHEA) was synthesized from polysuccinimide (PSI) through complete aminolysis by means of ethanolamine in DMF, and purified as previously reported (Giammona et al., 1987). 2-bromoisobutyryl bromide (BIBB), triethylamine (TEA), copper bromide (Cu^IBr), 2,2′-bipyridyl (Bpy), butyl methacrylate (ButMA), bis (4-nitrophenyl) carbonate (BNPC), polyvinylpyrrolidone 40 KDa (PVP), dimethylacetamide (DMA), dimethylformamide (DMF), methanol (MeOH), diethyl ether, HABA/Avidin Reagent, Dulbecco's phosphate buffer saline (DPBS), NaOH, HCl, biotin-dPEG®$_{11}$-NH_2 (PEG chain ≈ 500 Da), and sorafenib tosylate were purchased from Merck (Italy). SpectraPor dialysis tubing in regenerated cellulose was purchased from Spectrum Laboratories, Inc. (UK), while Minisart Syringe Filters were purchased from Sartorius (Germany). The ButMA stabilizing agent monomethyl ether hydroquinone was removed from the commercially available product through basic activated aluminium oxide column.

2.2. General methods

^1H NMR and ^{13}C NMR spectra were recorded using a Bruker Avance II 400 spectrometer operating at 400.15 and 100.63 MHz, respectively.

Size exclusion chromatography (SEC) analysis was carried out to determine weight average molecular weight (Mw) and polydispersity (PD) of each copolymer. The apparatus employed comprised a Phenomenex Phenogel 5 μm 10^4Å column connected to an Agilent 1260 Infinity Multi-Detector GPC/SEC system (Milan, Italy). Analyses were carried out at 50 °C using DMF + 0.1 M LiBr as a mobile phase at the flow rate of 0.8 mL/min and data were collected after absolute calibration of the instrument performed with a polystyrene standard (70 kDa).

2.3. Derivatization of PHEA with 2-bromoisobutyryl bromide (PHEA-g-BIB)

The PHEA-g-BIB copolymer was synthesized according to a previously reported protocol [24]. Briefly, 1 g of PHEA (6.2 mmol OH groups) was dissolved in anhydrous DMA (20 mL) at room temperature (RT). Then 880 μL of TEA were added, (molar ratio TEA: hydroxyl groups of PHEA set to 1:1) and the reaction mixture was cooled to 0 °C before the addition of 780 μL of BIBB (molar ratio BIBB: hydroxyl groups of PHEA of 1:1) while stirring vigorously. The flask content was allowed to react at RT for 4 h, after which the mixture was slowly dripped into cold diethyl ether. The precipitate was collected and washed twice with the same solvent, dried under reduced pressure, purified exhaustively by dialysis (MWCO 12–14 kDa) and finally lyophilized. ^1H NMR (300 MHz, DMF-d7, 25 °C) δ: 1.95 (s, 6H BIB, $(CH_3)_2$-C-CO-), 3.29 (m, 2H PHEA, –$NHCH_2CH2O$–), 3.58 (m, 2H PHEA, –$NHCH_2CH_2OH$), 4.25 (m, 2H PHEA, –$NHCH_2CH_2O$-BIB), 4.76 (m, 1H PHEA –NHCH(CO)CH_2–).

SEC: $\overline{M}_w = 67192$ (g/mol), $\overline{M}_n$=47994(g/mol), PD = 1.4.

2.4. ATRP polymerization of butyl methacrylate on PHEA-BIB (PHEA-g-IB-pButMA)

PHEA-g-IB-pButMA copolymer was obtained through Atom Transfer Radical Polymerization (ATRP) following an already established procedure (Giammona et al., 2022). Specifically, PHEA-g-BIB was dissolved in a pre-degassed mixture of 1:1 anhydrous DMF/MeOH (v/v) (300 mg, equivalent to 0.51 mmol of BIB, in 24 ml). Butyl methacrylate (800 μL) was thus added to the reaction flask, setting a molar ratio of 10 between the monomer and BIB. Subsequently, 71.6 mg of Cu^IBr catalyst (mol Cu^IBr/mol BIB equal to 1) and 312.36 mg of bipyridine (Bpy) (mol Bpy/mol Cu^IBr equal to 4) were blended with a spatula and then introduced into the flask, taking care to maintain continuous argon bubbling and vigorous stirring. The content was kept under an argon atmosphere at 50 °C and, after 20 h, the reaction was stopped by opening the flask. The isolation of the copolymer was assessed by slowly dripping the reaction mixture into water/MeOH 1:1, and the solid residue was washed twice with the same solvents. The obtained white solid was dissolved in DMF, purified by dialysis (MWCO 12–14 kDa), and retrieved as freeze-dried powder.

^{1}H NMR (300 MHz, DMF-d7, 25 °C, TMS) δ: 0.99 (m, 6H ButMA, –CH-CH_3 and –CH_2-CH_2-CH_3), 1.48 (m, 2H ButMA, –CH_2-CH_2-CH_3) 1.66 (m, 2H ButMA, –CH_2-CH_2-CH_3), 1.90 (s, 6H BIB, $(CH_3)_2$-C-CO-), 3.30 (m, 2H PHEA, –$NHCH_2CH_2O$–), 3.58 (m, 2H PHEA, –$NHCH_2CH_2OH$), 4.13 (m, 2H ButMA, (CO)-O-CH_2-CH_2-CH_2), 4.74 (m, 1H PHEA –NHCH (CO)CH_2–).

SEC: $\overline{M}_w = 399098$ (g/mol), $\overline{M}_n$=210052(g/mol), PD = 1.9.

2.5. Biotinylation of the copolymer: Synthesis of PHEA-g-IB-pButMA-g-PEG-Biotin

To obtain the biotinylated copolymer PHEA-g-IB-pButMA-g-PEG-Biotin, the butyl methacrylated derivative was conjugated with biotin-dPEG®$_{11}$-NH_2 using bis(4-nitrophenyl) carbonate (BNPC) as a coupling agent (Varvarà et al., 2024). First, 1 g of PHEA-g-IB-pButMA (1.45 mmol of repeating units) dissolved in 20 mL of aDMF, was added with 61 mg of BNPC in 2.5 mL of the same solvent (mol BNPC/mol repeating units: 0.08). The flask content was left to react for 4 h at 40 °C. On completion, 7.5 mL of a biotin-dPEG®$_{11}$-NH_2 solution in aDMF (20.56 mg mL^{-1}) were slowly added to the flask. After 18 h at 25 °C the mixture was dialyzed (MWCO 12–14 kDa) against basic water (NaOH) for 48 h and against ultrapure water for further 72 h. Lastly, the solution was lyophilized and stored as whitish powder.

^{1}H NMR (300 MHz, DMF-d7, 25 °C, TMS) δ: 0.99 (m, 6H ButMA, –CH-CH_3 and –CH_2-CH_2-CH_3), 1.48 (m, 2H ButMA, –CH_2-CH_2-CH_3) 1.66 (m, 2H ButMA, –CH_2-CH_2-CH_3), 1.90 (s, 6H BIB, $(CH_3)_2$-C-CO-), 3.29 (m, 2H PHEA, –$NHCH_2CH_2O$–), 3.58–3.6 (m, 2H PHEA, –$NHCH_2CH_2OH$; m, 45H PEG, –OCH_2CH_2O–), 4.13 (m, 2H ButMA, (CO)-O-CH_2-CH_2-CH_2), 4.74 (m, 1H PHEA –NHCH(CO)CH_2–).

^{13}C NMR (400 MHz, DMF-d7, 25 °C, TMS): 177.43 $(CO)_{BIB}$, 172.07–170.74 $(CO)_{PHEA}$, 71.39 $(–CH_2\text{-}O\text{-})_{PEG}$, 64.74 $(–CH_2\text{-}O\text{-})_{ButMA}$, 60.09 $(–CH_2\text{-}O\text{-})_{PHEA}$, 54.46 $(–CH\text{-}CO)_{PHEA}$, 45.77 $(–CH_2)_{ButMA}$, 44.94 $(–HN\text{-}CH_2\text{-})_{PHEA}$, 38.36 $(–CH_2\text{-}CO)_{PHEA}$, 19.5 $(–CH_3)_{ButMA}$, 13.61 $(–CH_3)_{ButMA}$.

SEC: $\overline{M}_w = 427398$ (g/mol), $\overline{M}_n$=213699(g/mol), PD = 2.

2.6. Preparation of nanoparticles by dialysis-based nanoprecipitation

To prepare polymeric nanoparticles, 100 mg of PHEA-g-IB-pButMA-g-PEG-Bt were solubilized in 50 ml of DMF. After complete dissolution, the copolymer solution was dialyzed against water (Visking Dialysis Tubing 18/32 '', 12–14,000 cut-offs in molecular weight) for one day against 2 L of ultrapure water for 24 h, replacing the external volume 5 times. After dialysis, 100 mg of polyvinylpyrrolidone (PVP) were added as cryoprotectant and the colloidal dispersion obtained was finally filtered through 5 µm membrane filter (Sartorius, Minisart Syringe Filter, Germany) and freeze-dried. This process allowed to gain both non targeted and biotinylated nanoparticles. To prepare sorafenib loaded nanoparticles, 63.5 mg of sorafenib tosylate were added to the organic phase (copolymer solution in DMF) before dialysis.

2.7. Nanoparticles characterization

The size distribution and Zeta-potential analyses were performed using a Malvern Zetasizer NanoZS instrument equipped with a 632 nm laser and a fixed scattering angle of 173° on 1 mL of sample (0.25 mg mL^{-1}). After size measurement, the sample was transferred to a Folded Capillary Zeta Cell and the Zeta-potential was determined through aqueous electrophoresis measurements at 25 °C, using the Smoluchowski relationship. The amount of entrapped drug was quantified after dissolution of 10 mg of nanoparticles in 0.5 mL of DMF. After few minutes, 4.5 mL of methanol were added, and the mixture was vigorously stirred for 3 h to extract the drug. The resulting suspension was filtered through syringe filter (0.2 µm R.C) and 50 µL of the resulting solution were injected to Agilent 1260 Infinity high-performance liquid chromatography (HPLC), equipped with a multiple wavelength detector, operating at 266 nm, and an Open Lab Chemstation software. The elution was carried out isocratically at 25 °C, using a reverse-phase Gemini C6-phenyl 110A column (Phenomenex 5 µm, 250 × 4.60 mm) and methanol/water 85:15 (v/v) mixture as a mobile phase with a flow rate of 1 mL min^{-1}. The drug loading (DL%) was expressed as the weight percent ratio between the loaded drug and the freeze-dried nanoparticles. The amount of surface exposed biotin on the nanoparticles surface, was investigated by HABA-avidin colorimetric assay. In brief, biotinylated nanoparticles were dispersed at a concentration of 1 mg mL^{-1} in ultrapure water and incubated with the HABA-avidin reagent following the manufacturer's instructions. UV readings were taken on filtered samples (syringe filter, cut-off 0.2 µm), and the amount of biotin was expressed as mol/mol percentage with respect to the repeating units of the copolymer. Nanoparticles were also analyzed by differential scanning calorimetry (DSC) coupled with thermal gravimetric analysis (TGA), using a DSC/TGA 131 EVO (by SETARAM Instruments). Each measurement was performed under nitrogen atmosphere with a flow of 1 mL min^{-1}, using 5 mg of dried sample placed into an alumina crucible. Samples were heated starting from 20 °C up to 500 °C, with a heating rate of 10 °C min^{-1}.

2.8. Drug release studies

For drug release experiments, 1 mL of nanoparticles in DPBS (corresponding to 0.25 mg of sorafenib tosylate) was placed into a dialysis tubing (12–14 kDa cut-off) against 9 mL DPBS pH 7.4 (enriched with 1 % Tween 80). At fixed time intervals, 0.2 mL of the receiving compartment was withdrawn and replaced with equal volume of fresh medium. To mimic oral administration, 1 mL of nanoparticles in water (corresponding to 0.25 mg of sorafenib tosylate) was placed into a dialysis tubing (12–14 kDa cut-off) against 9 mL of 0.1 M HCl for 2 h and then moved in DPBS pH 6.8 for further 22 h. Each experiment was stopped after 24 h and the drug released was quantified using HPLC analysis as described above, after dilution of each sample with 0.8 mL of MeOH.

2.9. In vitro studies

2.9.1. Cell cultures

The human HCC cell line HepG2 was obtained from the American Type Culture Collection (ATCC) (LGC Standards, Italy), and the HuH-7 cell line was provided by Merck (Italy). HepG2 cells were cultured in Roswell Park Memorial Institute (RPMI) medium (SIGMA, Milan, Italy), supplemented with 10 % (v/v) Fetal Bovine Serum (FBS) (GIBCO, Life Technologies, Monza MB, Italy), 2 mM l-glutamine, 100 U/mL penicillin–streptomycin and 1 mM sodium pyruvate (all reagents were from SIGMA). HuH-7 were maintained in Dulbecco's Modified Eagle Medium (DMEM) (GIBCO, Life Technologies) supplemented with 10 % (v/v) FBS and 100 U/mL penicillin–streptomycin. Cells were maintained in an atmosphere of 5 % CO2 and 95 % humified air at 37 °C.

2.9.2. Cell viability assay

Cell viability was determined using a 3-[4,5 dimethylthiazol-2-yl]-2,5-diphenyltetrazolium bromide (MTT) assay. Briefly, cells (5 × 10^3 cells/well) were plated in 96-well plates for 24 h. Subsequently, cells were grown for an additional 24, 48 or 72 h in presence of Bt-NPs@SOR, NPs@SOR, and free SOR, corresponding to sorafenib tosylate concentrations of 0.05 µM, 0.5 µM, 5 µM, 10 µM, 25 µM. At the end of treatment, the cells were washed twice with Dulbecco's phosphate-buffered saline (DPBS) pH 7.4 and incubated with medium containing MTT (Sigma-Aldrich, Milan, Italy). Following incubation for 3 h at 37 °C, the solution was removed, and DMSO was added for cell lysis and solubilization of the blue formazan crystals resulting from MTT reduction. Optical density of the supernatants was measured at 570 nm using a VarioskanTM Flash Multimode Reader (Thermo Fisher Scientific, Waltham, Massachusetts, USA). Cell viability was expressed as a percentage of living cells compared to the untreated control of seeded cells (taken as 100 %). The cytotoxic effect was also compared with that of empty nanoparticles at equivalent concentrations. All experiments were performed in triplicate.

2.10. *In vivo studies*

Eight-week-old male nude athymic mice (BALB/c nude CAnN.Cg-Foxn1nu/Crl) were obtained from Charles River Laboratories (Lecco, Italy) and allowed to acclimatize for one week under standard laboratory conditions. The mice were housed in temperature- and humidity-controlled rooms with a 12-hour light/dark cycle. Animal experiments were conducted in accordance with the ARRIVE guidelines and were conducted in compliance with both the European Community directive guidelines for the use of animals in laboratory (2010/63/EU) and Italian law (D.Lgs. 26/2014). The animal study protocol was approved by the Italian Ministry of Health (authorization n.506/2023-PR).

2.10.1. *Drug administration and experimental groups*

BALB/c nude mice were subcutaneously inoculated with 1x10^6 HuH-7 cells embedded in Matrigel (11573620, Corning) into the right flank. Once tumors reached a palpable size (about 300 mm^3), the mice were randomly assigned to six groups (6 mice per group): (i) BALB/c plus water (Veh); (ii) Balb/C plus 10 mg/kg/day of sorafenib tosylate (SOR); (iii) Balb/C plus empty nanoparticles (NPs); (iv) Balb/C plus 10 mg/kg/day sorafenib-loaded nanoparticles (NPs@SOR); (v) Balb/C plus empty targeted nanoparticles (Bt-NPs); (vi) Balb/C plus 10 mg/kg/day sorafenib-loaded targeted nanoparticles (Bt-NPs@SOR). Sorafenib tosylate was solubilised in DMSO and diluted 20 times with aqueous PVP 30 k 10 mg mL^{-1}.

The treatments were administered daily by oral gavage for 17 days. Tumor volumes and body weights were determined once a week, and tumor volume was measured using calibers and was calculated with the formula: $v = [\text{length} \times (\text{width})^2] \div 2$ (Cusimano et al., 2015). At the end of the treatment period, mice were euthanized via CO_2 inhalation and tumors were collected from each animal for further analysis.

2.10.2. *Hematoxylin and eosin (H&E) staining*

Tumor mass samples were fixed in 10 % neutral-buffered formalin (Bio-Optica) for 24 h. After overnight washing, tissue samples were dehydrated in graded ethanol and paraffin embedded. Sections of 4–6 μm in thickness were cut, mounted on silanized glass slides, and air-dried. To remove the paraffin, slides were immersed in xylene two times, for 3 min each; rehydrated with graded ethanol, 100 %, 95 %, 80 %, 70 %, and 50 %, for 3 min each; and transferred to tap water. After that, tissues were stained with H&E and morphological examination of the samples was performed. The mitotic count was assessed as the total number of mitotic cells per 10 high power fields (HPFs) at 20 × magnification using a Zeiss Axioplan light microscope (Carl Zeiss, Oberkochen, Germany).

2.10.3. *Immunohistochemistry (IHC)*

Mice were deeply anesthetized and intracardially perfused with ice-cold 4 % paraformaldehyde (PFA). Tumor mass specimens were fixed overnight in 10 % neutral-buffered formalin (Bio-Optica). After overnight washing, they were dehydrated in graded ethanol and paraffin-embedded taking care to preserve their anatomical orientation. Tissue sections of 5 μm were then cut, mounted on salinized glass slides and air dried. To remove the paraffin, slides were immersed in xylene two times, for 10 min each; rehydrated with graded ethanol, 100 %, 95 %, 70 %, and 50 %, two times for 10 min each; and transferred to distilled water. Antigens were retrieved in sodium citrate buffer (10 mM sodium citrate, 0.05 % Tween-20, pH 6.0) by microwave for 10 min, followed by rinsing with distilled water. Then, the slides were washed in PBS containing 0.025 % Tween-20 (PBS-T) twice for 5 min each, blocked in 5 % BSA/ 0.3 % PBST for 1 h at RT and incubated overnight at 4 °C with BSA 1 % with the following primary antibodies: mouse anti-CD31 (1:40, JC70A, DAKO, Glostrup, Denmark), mouse anti-Ki-67 (1:100, MIB-1; DAKO, Glostrup, Germany). Secondary biotinylated anti-mouse antibody was applied for 30 min at RT, followed by the avidin–biotin–peroxidase complex (Vector Laboratories, Burlingame, CA, USA) for 30 min at RT. The immunoreaction was then visualized by incubating the sections for 4 min in a 0.1 % 3,3-diaminobenzidine (DAB) and 0.02 % hydrogen peroxide solution (DAB substrate kit, Vector Laboratories, CA, USA). The sections were lightly counterstained with Mayer's hematoxylin (Histolab Products AB, Göteborg, Sweden) mounted in GVA mountant (Zymed Laboratories, San Francisco, CA, USA) and observed with a Zeiss Axioplan light microscope (Carl Zeiss, Oberkochen, Germany) fitted with a digital camera (AxioCam MRc5, Carl Zeiss). Immunohistochemical staining was analyzed by converting the images to 8-bit, and, using the appropriate threshold function, the percentage of positive area was measured (Varghese et al., 2014).

2.10.4. *Protein extraction*

Tissues were dissected in ice-cold Hank's balanced salt solution (HBSS: 137 mM NaCl, 5.4 mM KCl, 0.45 mM KH_2PO_4, 0.34 mM Na_2HPO_4, 4 mM, $NaHCO_3$, 5 mM glucose; pH 7.4) and stored at − 80 °C, until use. Tumor mass tissues were lysed in a lysis buffer containing 150 mN NaCl, 50 mM Tris–HCl (pH 7.5), 5 mM EDTA, 1 mM Na_3VO_4, 30 mM sodium pyrophosphate, 50 mM NaF, 1 mM acid phenyl-methyl-sulphonyl- fluoride, 5 mg mL^{-1} aprotinin, 2 mg mL^{-1} leupeptin, 1 mg mL^{-1} pepstatin, 10 % glycerol, and 0.2 % TritonTM X-100. Then, the homogenates were centrifuged at 14.000 rpm for 10 min at 4 °C. The protein concentration of the supernatant was determined by the Bradford method (Bradford, 1976).

2.10.5. *Western blot analysis*

Equal amounts of proteins (50 μg) were separated by 8 %–15 % SDS-PAGE gels and transferred onto Hybond ECL nitrocellulose membranes (10600003, Amersham Life Science, Buckinghamshire, UK). Membranes were blocked with 5 % non-fat dry milk (Bio-Rad Laboratories, Segrate, Italy) in phosphate-buffered saline plus 0.05 % Tween 20 (PBS-T) for 1 h at RT, and were then probed overnight at 4 °C on orbital shaker with the following primary antibodies: mouse anti-AKT (1:1000, #2920, Cell Signaling, Danvers, Massachusetts, USA), rabbit anti-phospho-AKT (1:1000, #9271, Cell Signaling), rabbit anti-phospho-p38 (1:500, #9211, Cell Signaling), rabbit anti-p38 (1:500, #9212, Cell Signaling), rabbit anti-Casp-8 (1:500, #ab49853, abcam). Then, the membranes were washed 3 times with PBS-T and probed with the appropriate horseradish peroxidase-conjugated secondary antibodies (sheep anti-mouse NXA931V, Amersham Life Science, donkey anti-rabbit NA934V, Amersham Life Science) for 1 h at RT in 5 % non-fat dry milk. After washing with PBS-T, protein bands were visualized using enhanced chemiluminescence (ECL) (Thermo Fisher Scientific, Inc, Massachussets, United States of America) and scanned using the iBright FL1500 Imaging System (Thermo Fisher Scientific). Densitometric analysis of band intensity was performed with the aid of ImageJ software version 1.53v (developed by NIH, freeware, available online: https://imagej.nih.gov/ij/).

2.11. *Statistical analysis*

Data are presented as mean ± SEM and were analyzed using the one-way ANOVA test, followed by the Tukey post-hoc test for multiple comparisons. Unless otherwise stated, statistical significance was set at a $p < 0.05$. Statistical analyses were performed using Graph Pad Prism (Ver. 8, La Jolla, CA, USA).

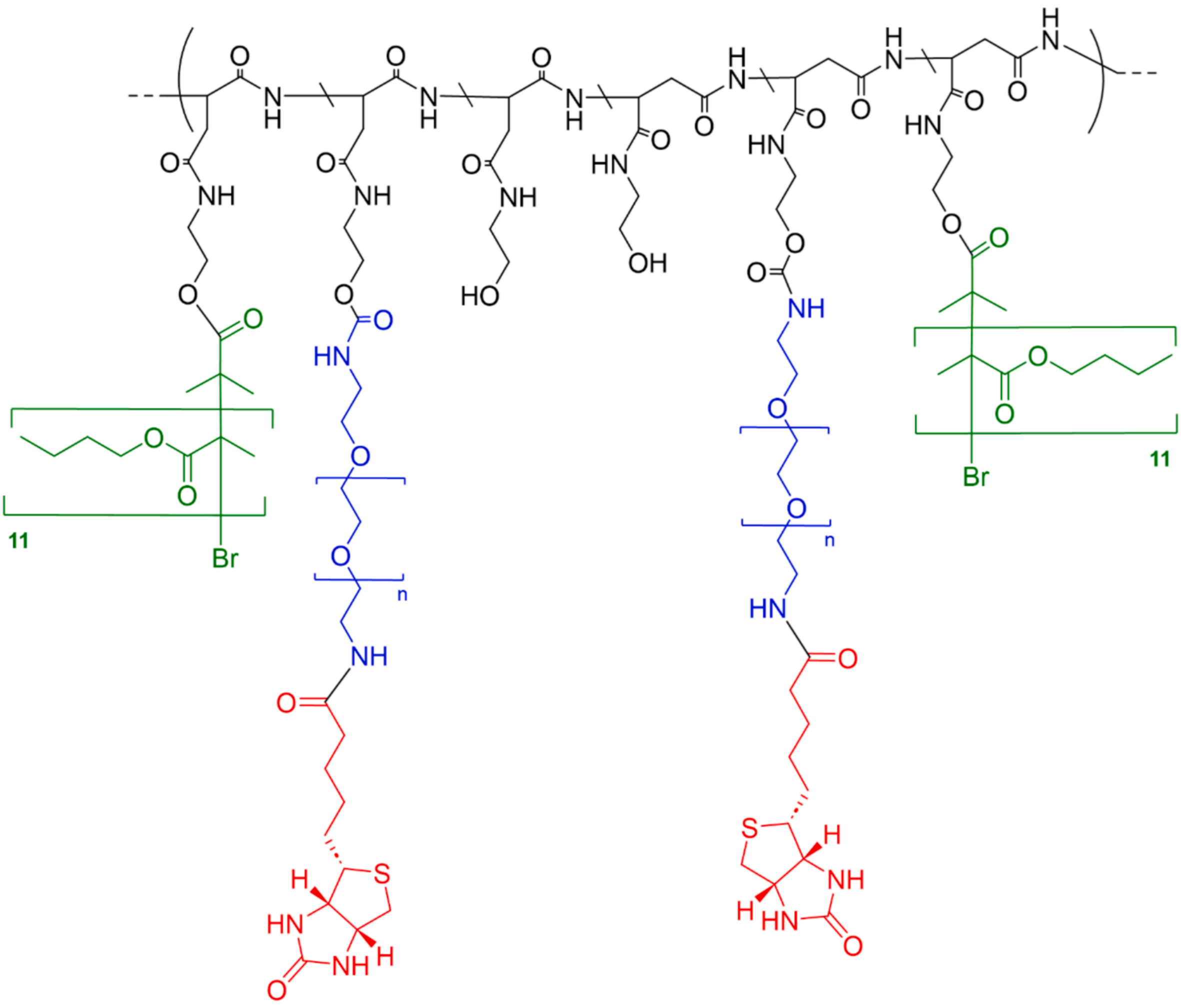

Fig. 1. Structure of PHEA-g-IB-pButMA-g-PEG-Bt.

Table 1

Values of molar derivatization degrees (DD %) calculated by ^{1}H NMR analyses, weight average molar weight (Mw) and polydispersity (Đ) determined through SEC analysis.

Derivative	DD$_{BIB}$%	DD$_{ButMA}$%	DD$_{PEG}$%	$\overline{M_w}$	Đ
PHEA	–	–	–	45,446	1.4
PHEA-g-BIB	35	–	–	67,192	1.7
PHEA-g-IB-pButMA	35	385	–	399,098	1.9
PHEA-g-IB-pButMA-g-PEG-Bt	35	385	7	427,398	2.0

3. Results and discussion

3.1. *Synthesis and characterization of the copolymer PHEA-g-IB-pButMA-g-PEG-Bt*

The amphiphilic grafted copolymer, designed to generate nanoparticles capable of efficiently loading the antineoplastic drug sorafenib, was synthesized through a controlled polymerization approach. Atom Transfer Radical Polymerization (ATRP) was chosen as polymerization method for its ability to precisely control chain growth, enabling the creation of tailored polymer structures. Previous studies have demonstrated that the synthesis of amphiphilic graft copolymers, consisting of hydrophilic α,β-poly(N-2-hydroxyethyl)-D,L-aspartamide (PHEA) backbone and hydrophobic poly(butyl methacrylate) (PBMA) side chains obtained via atom transfer radical polymerization (ATRP), facilitates the production of nanoparticles with enhanced efficacy for the targeted delivery of sorafenib to hepatocarcinoma cells. [24]. The features of this copolymer were thus further widened by attaching biotin as active targeting ligand towards cancer cells with high proliferation rate, such as hepatocarcinoma, which typically overexpress biotin receptors on their membrane. The final graft copolymer PHEA-g-IB-(pButMA)-g-PEG-Bt (Fig. 1) was prepared via a three-step synthesis (**Fig. S1**). First, the macroinitiator PHEA-BIB was obtained by reacting PHEA hydroxyl groups with the acyl bromide 2-bromoisobutyryl bromide (BIBB) using triethylamine as catalyst. ^{1}H NMR analysis allowed to calculate the BIB derivatization degree (DD%) comparing the integral of the peak related to the methyl groups of BIB (δ 1.95 ppm) with that assigned to CH$_2$ of the PHEA (δ 3.29 ppm), resulting in a DD% of 35 mol% (Table 1, **Fig. S2**). The hydrophilic macroinitiator PHEA-BIB was then isolated and used as reactive backbone to perform ATRP of butyl methacrylate (ButMA) monomers. This second step of the synthetic route led to the amphiphilic copolymer PHEA-g-IB-pButMA. ^{1}H NMR spectrum of the copolymer showed a DD% in ButMA equal to 385 mol%, calculated by analyzing the integral of the peak of the methyl groups of ButMA (δ 0.99 ppm) in comparison with that attributed to the methylene group of PHEA (δ 3.30 ppm) (Table 1, **Fig. S3**). Taking into account the already calculated DD% in BIB of 35 mol%, the polymerization extension (n: derivatization degree in ButMA/derivatization degree in BIB) of ButMA was quantified to be 11. Finally, the last step of the synthetic pathway involved the functionalization of the graft copolymer PHEA-g-IB-pButMA via carbonate ester with biotin residues already linked to a polyethylene glycol spacer, leading to the carbamate linkage between the hydroxyl group of

Table 2
Physico-chemical characterizations of sorafenib nanoparticles.

	Z-Average (nm)	*PDI*	Z-Potential (mV)	Drug Loading (% w/w)	Biotin Content (mol/mol%)
NPs@SOR	310 ± 16	0.241 ± 0.05	−24.3 ± 5.1	6.1 ± 1.2	–
Bt-NPs@SOR	330 ± 21	0.217 ± 0.02	−25.4 ± 6.1	8.4 ± 1.6	1.5

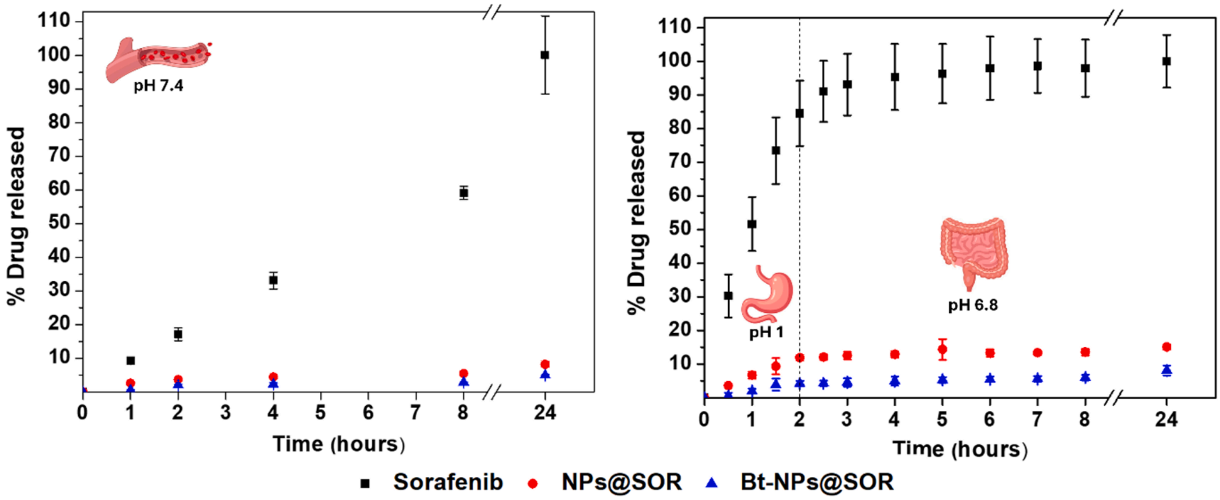

Fig. 2. Percentage of sorafenib released from NPs@SOR and Bt- NPs@SOR, compared with dissolution of free drug, under physiological conditions, simulating parenteral administration (pH 7.4 at 37 °C, 24 h) or oral administration (pH 1 at 37 °C, 2 h; pH 6.8 at 37 °C, 22 h).

the PHEA backbone and the free amino group of the pegylated targeting agent. The targeted copolymer PHEA-g-IB-pButMA-g-PEG-Bt was analyzed by ^{1}H NMR spectroscopy calculating a PEG DD% of 7 mol% comparing the integral of the peak of the methylene groups of PEG (δ 3.58 ppm) with that attributed to the methylene group of PHEA (δ 3.29 ppm) (Table 1, **Fig. S4**). Moreover, ^{13}C NMR spectroscopy confirmed the functionalization, as visible from the new peak at δ 71.39 referred to the conjugation polyethylene glycol (**Fig. S5**). All the synthesized copolymers were characterized using SEC analysis to determine the weight average molar weight ($\overline{M}_w$) and polydispersity ($\overline{M}_w$ / $\overline{M}_n$) registering the data summarized in Table 1. The results indicated an increase in molecular weight that aligns with the sequential derivatization steps conducted. These findings indicate successful synthesis and functionalization of the targeted copolymer for drug delivery applications.

3.2. Preparation and characterization of sorafenib loaded polymeric nanoparticles

Sorafenib loaded nanoparticles were prepared by dialysis-based nanoprecipitation, where the slow diffusion of the organic solvent through a dialysis membrane leads to nanoparticles formation. The obtained nanoparticles were characterized in terms of size distribution, Zeta-potential, drug loading and surface-exposed biotin content. A summary of the listed characterizations is provided in Table 2.

Both samples of sorafenib-loaded nanoparticles displayed dimensions of approximately 300 nm and possess similar surface charge, showing that the functionalization with biotinylated PEG$_{400}$, does not alter the aggregation of polymer chains during the nucleation and growth phase of the particle formation process. These dimensions are suitable for both oral and parenteral administration, also allowing, through passive targeting, greater accumulation in the liver (Song et al., 2014), where, especially in cases of HCC, the epithelium is largely fenestrated (Yuan et al., 1995). About the potential risk of NPs at ~ 300 nm, rapid clearance from the plasma circulation is generally reported, precisely because of increased hepatic accumulation (Song et al., 2014), which in the case of hepatic cancer treatment can be a benefit rather than a drawback. Additionally, 300 nm nanoparticles are not generally associated with vascular occlusion, as vascular blockage is reported to occur with particles larger than 10 μm (Hu et al., 2019).

Furthermore, the presence of biotin on the nanoparticle surface suggests that the nanoprecipitation by dialysis allows an adequate exposure of the biotin-functionalized PEG, making them potentially effective for targeted drug delivery.

In terms of amount of entrapped drug, only a slight increase in drug content was observed in the biotinylated nanoparticles (8.4 %) compared to non-targeted ones (6.1 %). By DSC analyses (**Figs. S6-S7**) it was not possible to clearly distinguish the peaks related to the fusion of the free sorafenib after incorporation, suggesting that the drug was presumably located within the inner core of nanoparticles as a molecular dispersion. These results suggest that the synthesis protocol used yields nanoparticles potentially able to deliver efficiently sorafenib to the tumor target. Additionally, stability studies conducted through DLS analyses over a period of up to one-month period, showed that the biotinylated sorafenib-loaded nanoparticles retain nearly unchanged characteristics after being stored as a lyophilized powder at 4 °C or 25 °C (**Table S1**). Similar stability results were obtained for not biotinylated sorafenib loaded nanoparticles.

3.3. Drug release studies

The ability of nanoparticles to release the entrapped drug in a controlled manner was assessed under physiological conditions, simulating parenteral administration (pH 7.4 at 37 °C, 24 h) or oral administration (pH 1 at 37 °C, 2 h; pH 6.8 at 37 °C, 22 h).

As shown in Fig. 2, independently by the condition analyzed, both targeted and non-targeted nanoparticles avoid any potentially problematic burst effect, as they show a very slow drug release, which does not exceed 15 % of the total drug trapped after 24 h. However, it might be noticed that sorafenib is released slower when incorporated in the targeted nanoparticles under conditions mimicking oral administration

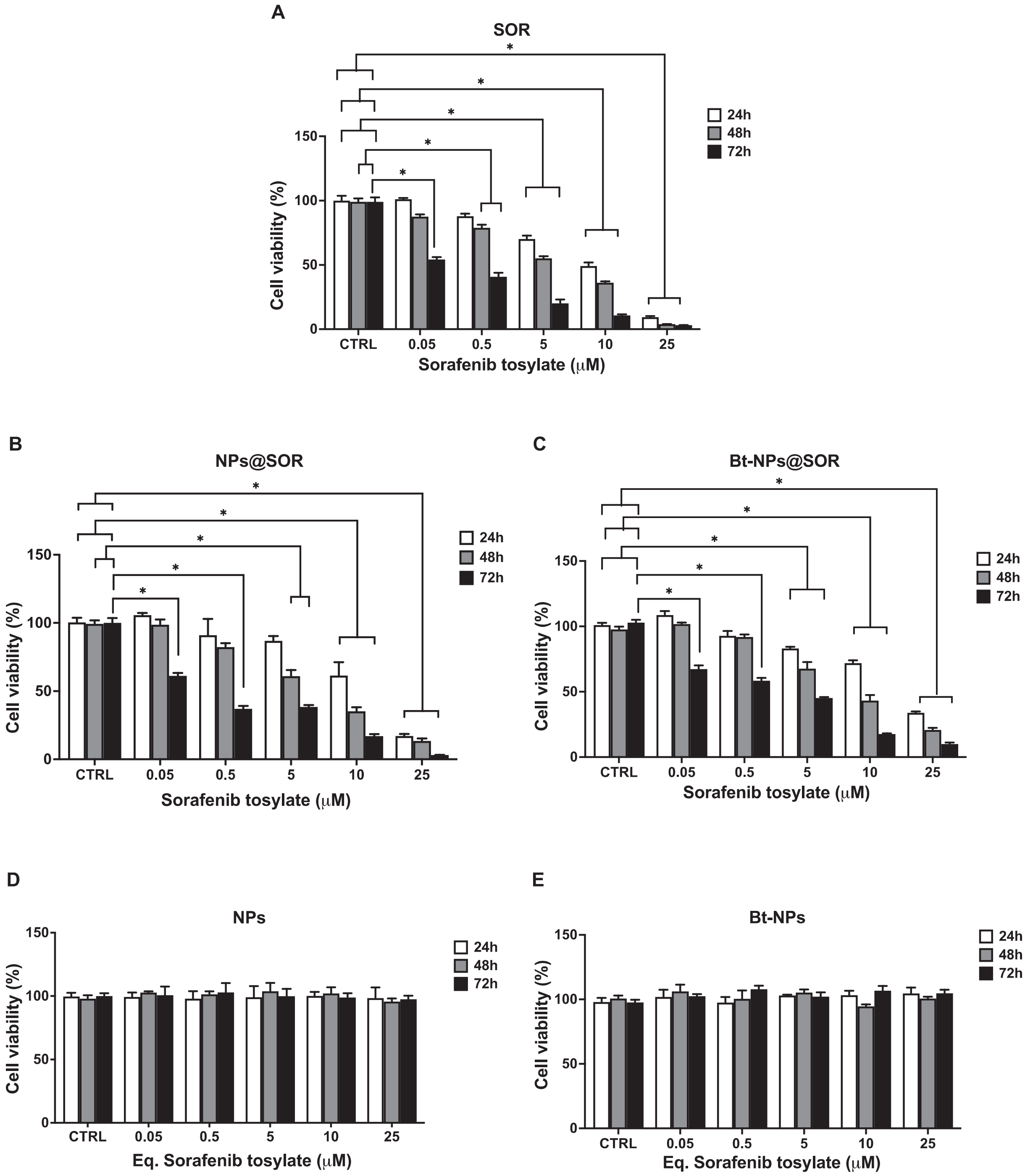

Fig. 3. Concentration-related (range 0.05μM-25μM) effect of (A) SOR, (B) NPs@SOR, (C) Bt-NPs@SOR, (D) NPs and (E) Bt-NPs upon HepG2 cells viability (%) following 24, 48, and 72h treatment. The data are expressed as means ± S.E.M. One-way ANOVA and the Tukey post-hoc test were used to determine statistical significance. *p < 0.05.

Table 3
IC50 average values for free sorafenib (SOR), sorafenib-loaded nanoparticles (NPs@SOR) and sorafenib-loaded biotin-conjugated polymeric nanoparticles (Bt-NPs@SOR) in HepG2 hepatocellular carcinoma cells after 24, 48, and 72 h of treatment.

HepG2 cell line	SOR	NPs@SOR	Bt-NPs@SOR
IC50 (μM) – 24 h	7.3 (5.3 to 9.1)	9.0 (7.6 to 10.6)	9.1 (7.1 to 11.5)
IC50 (μM) – 48 h	3.0 (1.9 to 4.8)	5.8 (4.0 to 7.0)	5.7 (3.4 to 7.1)
IC50 (μM) – 72 h	1.7 (1.3 to 2.7)	3.0 (1.6 to 5.4)	4.8 (3.0 to 5.8)

(15 % vs 7 % after 24 h). This can be ascribed to a more collapsed polymeric shell due to PEG chains on the surface. This type of release profile appears to be potentially advantageous for chemotherapy, as it could reduce the frequency of administration. Furthermore, nanoparticles with a long circulation time, such as stealth particles, would thus have enough time to accumulate onto the target site without losing their load prematurely in the systemic circulation or in the transit compartments (i.e. gastrointestinal tract), thereby minimizing the occurrence of side effects.

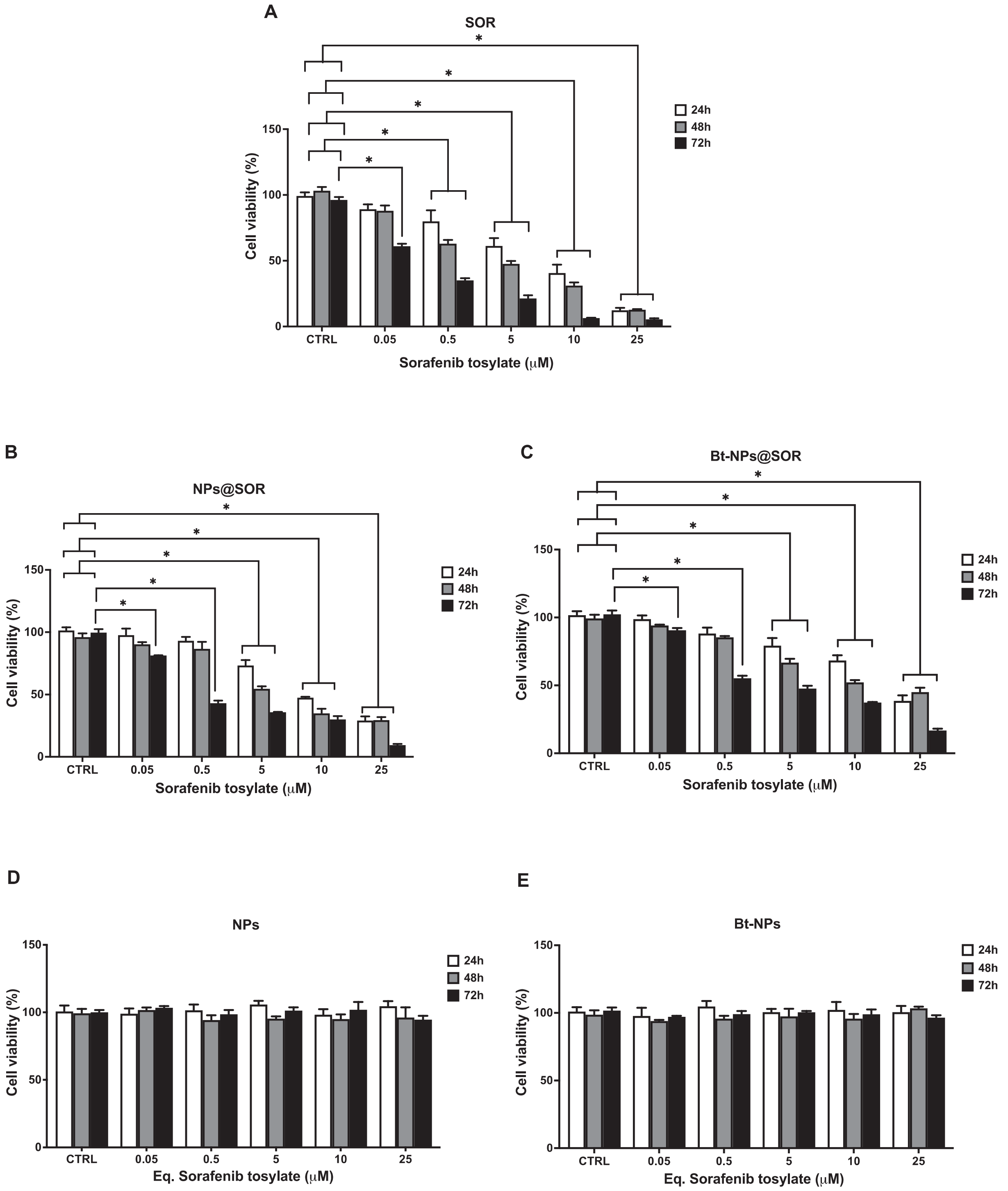

Fig. 4. Concentration-related (range 0.05 μM-25 μM) effect of (A) SOR, (B) NPs@SOR, (C) Bt-NPs@SOR, (D) NPs and (E) Bt-NPs upon HuH-7 cells viability (%) following 24, 48, and 72 h treatment. The data are expressed as means ± S.E.M. One-way ANOVA and the Tukey post-hoc test were used to determine statistical significance. $^{*}p < 0.05$.

3.4. Effects of sorafenib-loaded polymeric nanoparticles on viability of HepG2 cells

The Fig. 3 presents the results of the HepG2 cell viability assay, demonstrating the effects of SOR, NPs@SOR, and Bt-NPs@SOR on HepG2 cells over 24, 48, and 72 h.

The graphs presented in Fig. 3 revealed that all treatments with sorafenib, free or encapsulated in nanoparticles, result in progressive decrease of HepG2 cell viability, with more pronounced effects at higher concentrations and longer exposure times.

However, SOR consistently exhibits the highest potency among the treatments, as evidenced by its steeper dose–response curves and lower IC50 values across all time points. The IC50 values, presented in Table 3, quantitatively confirm these observations. For SOR, the IC50 values at 24, 48, and 72 h were 7.3 μM (5.3 to 9.1), 3.0 μM (1.9 to 4.8), and 1.7 μM (1.3 to 2.7), respectively. These values demonstrate a clear time-dependent increase in potency, consistent with previous findings on sorafenib's cytotoxic effects on HepG2 cells (Giammona et al., 2022;

Table 4
IC50 average values for free sorafenib (SOR), sorafenib-loaded nanoparticles (NPs@SOR) and sorafenib-loaded biotin-conjugated polymeric nanoparticles (Bt-NPs@SOR) in HuH-7 hepatocellular carcinoma cells after 24, 48, and 72 h of treatment.

HuH-7 cell line	SOR	NPs@SOR	Bt-NPs@SOR
IC50 (μM) – 24 h	6.9 (4.9 to 8.7)	6.7 (6.2 to 7.4)	8.2 (5.9 to 10.5)
IC50 (μM) – 48 h	2.2 (1.3 to 3.6)	3.6 (2.4 to 4.8)	4.0 (2.3 to 5.9)
IC50 (μM) – 72 h	0.8 (0.5 to 1.4)	1.1 (0.5 to 2.1)	1.3 (0.5 to 2.5)

Llovet et al., 2008). NPs@SOR showed slightly higher IC50 values of 9.0 μM (7.6 to 10.6), 5.8 μM (4.0 to 7.0), and 3.0 μM (1.6 to 5.4) at the same time points. Bt-NPs@SOR exhibited IC50 values of 9.1 μM (7.1 to 11.5), 5.7 μM (3.4 to 7.1), and 4.8 μM (3.0 to 5.8). These findings are linked to the ability of polymeric nanoparticles to release the loaded drugs gradually, as demonstrated by drug release studies and supported by previously literature (Wilhelm et al., 2016).

3.5. *Effects of sorafenib loaded polymeric nanoparticles on viability of HuH-7 cells*

The Fig. 4 presents data for cytotoxicity evaluation on the HuH-7 cell line, providing a comparison of treatment effects between two different HCC cell lines. Similarly to HepG2 cells, a clear dose- and time-dependent reduction in cell viability was shown for HuH-7 cells for all treatments. However, the bar graphs for HuH-7 cells appear to be shifted towards lower concentrations compared to HepG2 cells, suggesting a higher sensitivity of HuH-7 cells to these treatments. This is particularly evident at the 72-hour time point, where the cell viability is notably lower for all treatments in HuH-7 cells. The IC50 values shown in Table 4 for HuH-7 cells further confirm their increased sensitivity to the treatments. For SOR, the IC50 values at 24, 48, and 72 h were 6.9 μM (4.9 to 8.7), 2.2 μM (1.3 to 3.6), and 0.8 μM (0.5 to 1.4), respectively. NPs@SOR showed IC50 values of 6.7 μM (6.2 to 7.4), 3.6 μM (2.4 to 4.8), and 1.1 μM (0.5 to 2.1), while Bt-NPs@SOR exhibited IC50 values of 8.2 μM (5.9 to 10.5), 4.0 μM (2.3 to 5.9), and 1.3 μM (0.5 to 2.5) at the same time points. Interestingly, in HuH-7 cells, the difference in potency between SOR and the other two treatments appears to be less pronounced than in HepG2 cells, particularly at the 24-hour time point. This suggests that the relative efficacy of these treatments may vary depending on the specific characteristics of the HCC cell line.

3.6. *Anticancer effects of sorafenib-loaded biotin-conjugated polymeric nanoparticles in vivo*

A mouse xenograft tumor model of HuH-7 cells was used to assess the in vivo efficacy of sorafenib-loaded biotin-conjugated polymeric nanoparticles on HCC. When tumors became palpable, at a size of about 300 mm^3, mice were randomized into six groups of six animals each. Each group was treated for 17 days with free sorafenib (SOR), vehicle (water), sorafenib containing NPs (NPs@SOR), sorafenib-loaded biotin-conjugated polymeric nanoparticles (Bt-NPs@SOR), empty NPs (as a control of NPs@SOR) and empty Bt-NPs (as a control of Bt-NPs@SOR). The SOR, NPs@SOR and Bt-NPs@SOR treated groups received the drug at 10 mg kg^{-1} daily oral (p.o.) gavage, while the other three groups received water or empty nanoparticles at equivalent concentration. At regular time intervals (0, 7, 14, and 21 days) tumor volumes (Fig. 5B) and body weight (Fig. 5C) were recorded, and the results were expressed in function of time.

Fig. 5A, shows images of mice and their respective tumors at the end of the 17 days treatment, acquired by using a digital photo camera, were reported and they are representative of all collected tumors.

The results presented in Fig. 5 provide a comprehensive demonstration of the superior in vivo antitumor efficacy of biotin-functionalized nanoparticles loaded with sorafenib (Bt-NPs@SOR) compared to both non-functionalized nanoparticles (NPs@SOR) and free sorafenib. This enhanced efficacy can be attributed to several synergistic factors. First, the biotin-mediated active targeting likely facilitated preferential accumulation of the nanoparticles in tumor tissue, exploiting the overexpression of biotin receptors on hepatocellular carcinoma cells (Chen et al., 2019; Varvarà et al., 2024). In addition, the PEGylation of the nanoparticle surface contributed to prolonged systemic circulation and reduced clearance, allowing for sustained drug release and increased tumor exposure to sorafenib (Varvarà et al., 2024; Wang et al., 2022). The slow and controlled release profile, as demonstrated in the drug release studies, minimized premature drug loss and maintained therapeutic concentrations at the tumor site, which is critical for maximizing the antitumor effect while reducing systemic toxicity.

Furthermore, the absence of significant body weight loss across all treatment groups (Fig. 5C) suggests that the nanoparticle formulations, particularly Bt-NPs@SOR, did not induce notable systemic toxicity, supporting the safety and tolerability of this approach. This is particularly relevant given the well-documented adverse effects associated with free sorafenib therapy (Abdel-Rahman and Lamarca, 2017).

These findings are consistent with previous reports indicating that targeted nanocarriers can overcome several limitations of conventional chemotherapy, including poor tumor selectivity, rapid drug clearance, and off-target side effects (Böttger et al., 2020; Varvarà et al., 2024; Wilhelm et al., 2016).

The observed divergence between in vitro and in vivo efficacy of Bt-NPs@SOR stems from fundamental differences between experimental models and biological environments. While in vitro assays showed comparable cytotoxicity for Bt-NPs@SOR and NPs@SOR, as demonstrated by overlapping IC50 confidence intervals (Tables 3-4), in vivo studies revealed a marked superiority of Bt-NPs@SOR in suppressing tumor growth (Fig. 5). This discrepancy can be explained by the sustained release profile of Bt-NPs@SOR, which limits immediate drug availability in short-term in vitro assays but allows for gradual and prolonged accumulation in tumors in vivo, thanks to the enhanced permeability and retention (EPR) effect and biotin-mediated active targeting. Moreover, the tumor microenvironment in vivo, characterized by biotin receptor overexpression on hepatocellular carcinoma cells (Chen et al., 2019), facilitates receptor-mediated uptake of Bt-NPs@SOR a mechanism absent in 2D in vitro models, which lack the complexity needed for efficient targeting. PEGylation further supports this process by reducing protein corona formation and extending systemic circulation (Wang et al., 2022). Notably, conventional 2D cultures fail to replicate the structural and functional complexity of tumors, including interstitial fluid pressure and extracellular matrix density, which are crucial for nanoparticle penetration and retention. Methodological studies (Seidu et al., 2022) confirm that 2D systems often underestimate the efficacy of targeted nanocarriers. Such results highlight the limitations of 2D in vitro models, which cannot accurately mimic the complexity of the in vivo tumor microenvironment and therefore may underestimate the efficacy of targeted nanosystems.

To further elucidate the mechanisms underlying the observed antitumor effects, we next examined histological and immunohistochemical markers of proliferation and angiogenesis in tumor tissues from the different treatment groups. The histological analysis of tumor sections stained with hematoxylin-eosin (Fig. 6A) shows consistent morphological changes across SOR, NPs@SOR, and Bt-NPs@SOR in vivo. The antiproliferative and antiangiogenic effects of free sorafenib and sorafenib encapsulated in NPs were assessed through immunohistochemical analyses. Specifically, to evaluate the antiproliferative effects of the different treatments, the expression levels of the nuclear proliferation marker Ki-67 were examined. Animals treated with Bt-NPs@SOR displayed a significantly reduced Ki-67 positive staining area compared to those treated with the vehicle, free drug, empty nanoparticles, or NPs@SOR, indicating that tumor cell proliferation was most effectively suppressed by sorafenib loaded into targeted nanoparticles (Fig. 6B).

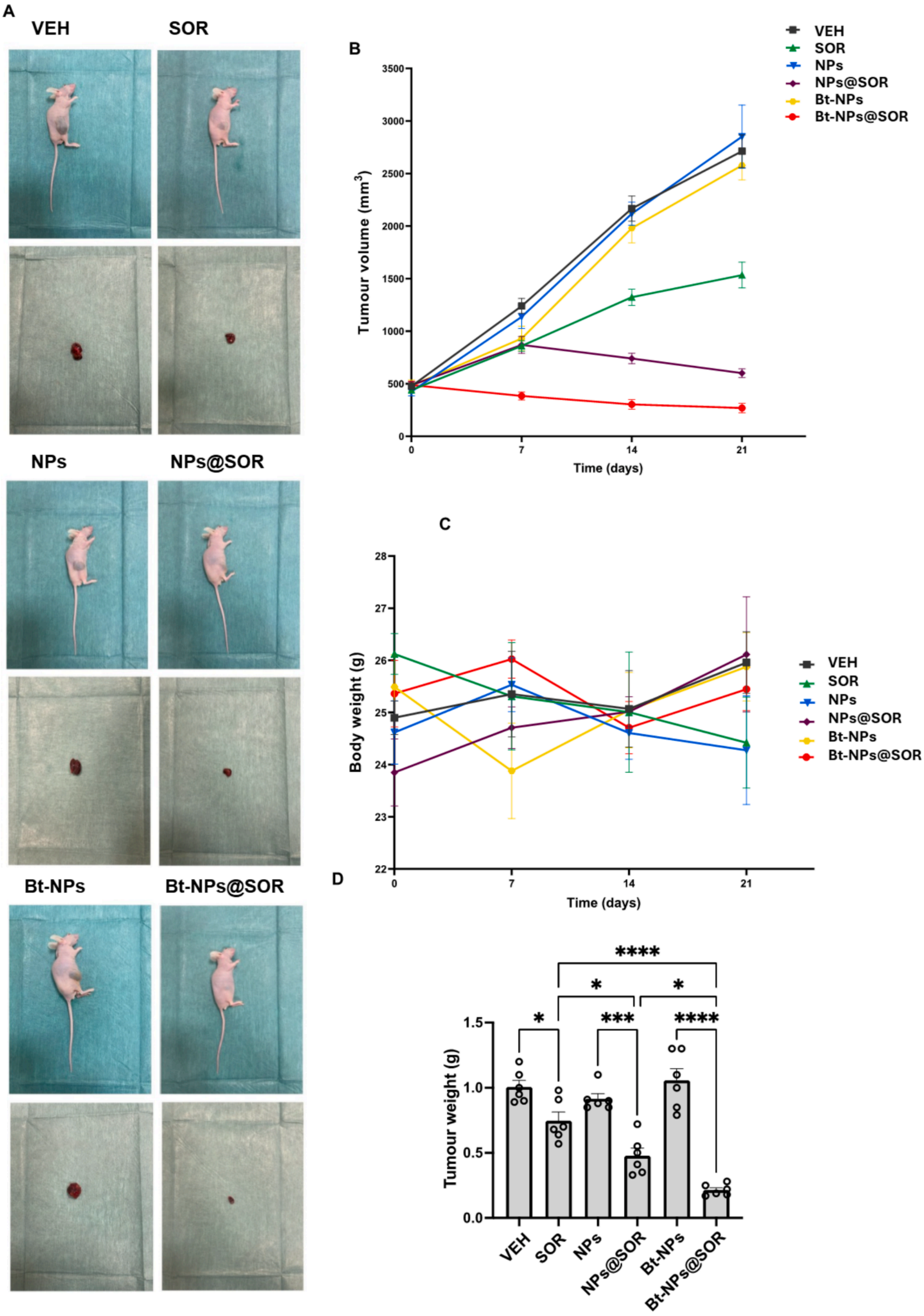

Fig. 5. In vivo therapeutic efficacy of sorafenib-loaded biotin-conjugated polymeric nanoparticles on xenograft models of HuH-7 cells (n = 6 mice per group). (A) The ex vivo optical images of tumors, (B) tumor volume, (C) mice body weights after 0, 7, 14 and 21 days. (D) Tumor dimension reduction at the end of the 17 days treatment. The data are expressed as means ± S.E.M. One-way ANOVA and the Tukey post-hoc test were used to determine statistical significance. *$p < 0.05$, ***$p < 0.001$, ****$p < 0.0001$.

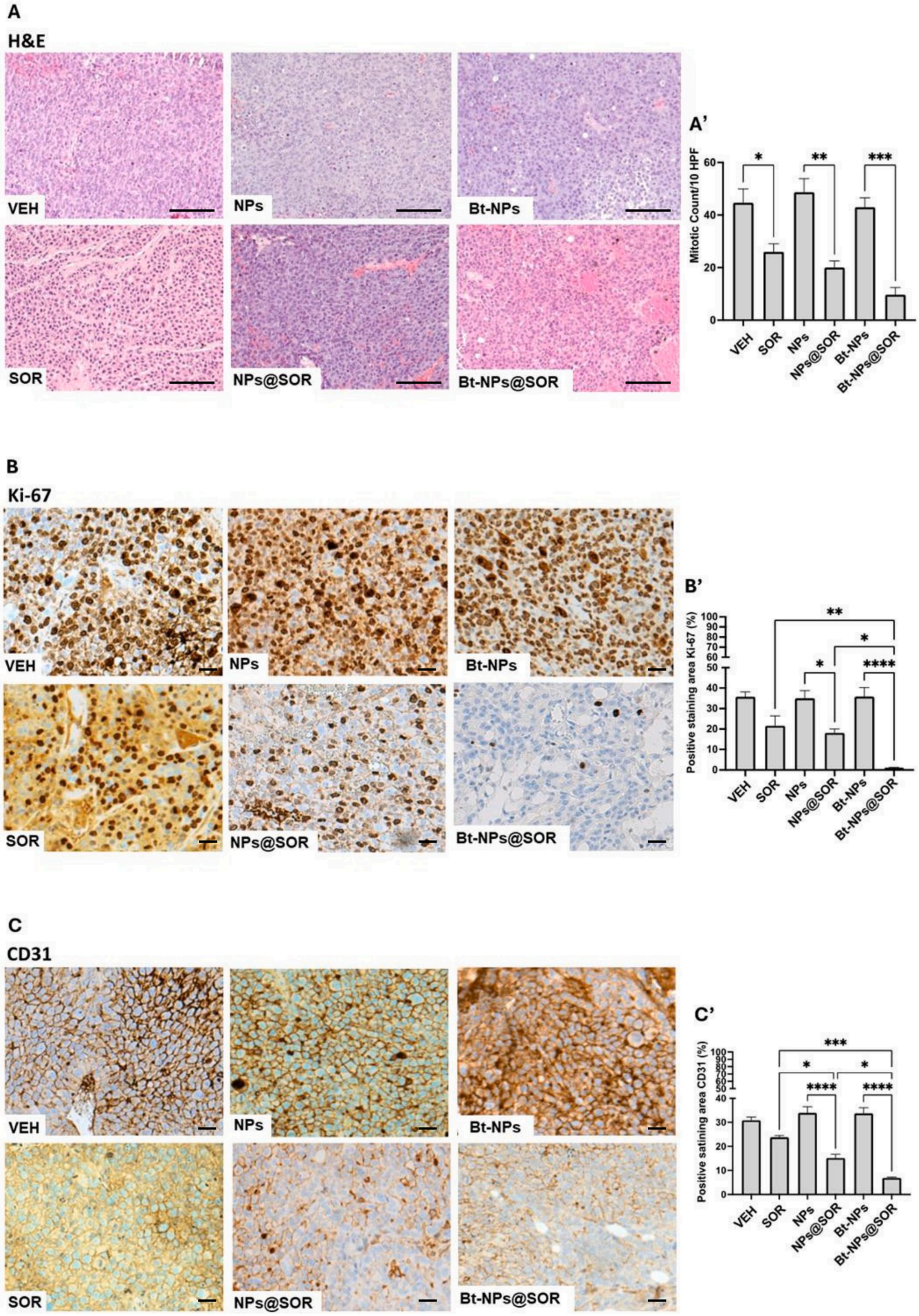

Fig. 6. (A) Representative H&E staining of tumor samples from Huh7 xenograft models (n = 3 mice per group; H&E; original magnification 200x; scale bar = 50 µm). (A') Mitotic count quantification expressed as mitoses/10 high-power fields (HPF). (B) Immunohistochemical staining of tumor samples for evaluation of Ki-67 proliferation index (immunoperoxidase; original magnification 400x; scale bar = 10 µm). (B') Quantitative assessment of Ki-67-positive nuclear area. (C) CD31 staining of blood vessels in tumor samples (immunoperoxidase; original magnification 400x; scale bar = 10 µm). (C') Quantification of CD31-positive vascular structures. The data are expressed as means ± S.E.M. One-way ANOVA and the Tukey post-hoc test were used to determine statistical significance. $^{*}p < 0.05$, $^{**}p < 0.01$, $^{***}p < 0.001$, $^{****}p < 0.0001$.

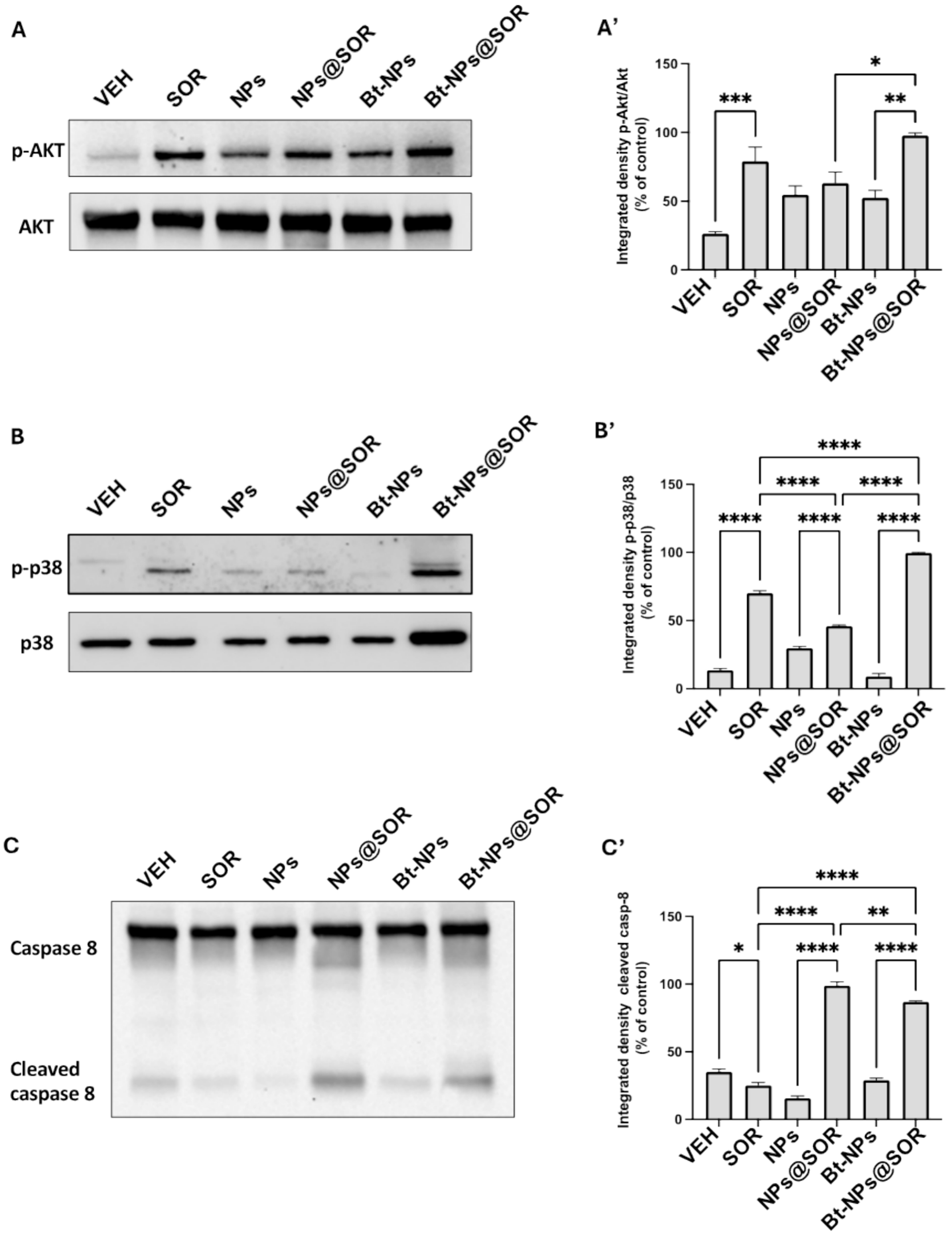

Fig. 7. Western blot analysis of key signaling pathways in tumor samples from Huh7 xenograft models (n = 3 mice per group). Left panels (A, B, C) show representative Western blots for p-AKT/AKT, p-p38/p38, and Caspase 8/Cleaved caspase 8 across different treatments (VEH, SOR, NPs, NPs@SOR, Bt-NPs, Bt-NPs@SOR). Right panels (A', B', C') show densitometric quantification of protein levels normalized to controls (expressed as percentage of control). The data are expressed as means ± S.E.M. One-way ANOVA and the Tukey post-hoc test were used to determine statistical significance. $^*p < 0.05$, $^{**}p < 0.01$, $^{***}p < 0.001$, $^{****}p < 0.0001$.

The data corroborate that sorafenib can suppress tumor proliferation in vivo by impeding cell cycle progression, which aligns with prior reports in gastrointestinal and liver cancers (Basilio-de-Oliveira and Pannain, 2015; Yang et al., 2018). The lowest Ki-67 levels in Bt-NPs@SOR treated tissues suggest that improved drug concentration in the tumor microenvironment intensifies antiproliferative activity over standard formulations, consistent with biotin-driven uptake mechanisms (Ma et al., 2021; Zhang et al., 2022). Furthermore, the tumor vasculature was assessed in tumor samples through CD31 staining of blood vessels (Fig. 6C). Similarly, to Ki-67 positive staining, the quantity of CD31-positive cells showed a substantial increase in tumors from mice treated with both vehicle and empty nanoparticles. In contrast, tumor samples obtained from mice treated with Bt-NPs@SOR exhibited a marked reduction in CD31-positive cells (Fig. 6C), suggesting that the tumor-suppressive effect of sorafenib entrapped into targeted nanoparticles may be driven by vascular disruption. The notable CD31 reduction with Bt-NPs@SOR reflects the intensification of anti-angiogenic effects, likely due to higher local drug availability, mirroring reports of advanced formulations adding to the blockade of tumor neovascularization (Ma et al., 2021; Romualdo et al., 2021; Zhang et al., 2022). Collectively, these experimental findings provide compelling evidence for the enhanced therapeutic effectiveness of sorafenib when delivered through polymeric nanoparticles.

To assess changes in the expression of molecular markers following the different treatments, protein extracts from tumors harvested from treated mice were subjected to Western blot analysis (Fig. 7). The AKT pathway analysis shows differential phosphorylation patterns across treatments. Bt-NPs@SOR treatment induced the highest p-AKT/AKT ratio, followed by SOR and NPs@SOR, while vehicle control showed minimal activation (Fig. 7A). This suggests enhanced activation of the AKT survival pathway, particularly with Bt-NPs@SOR treatment. The enhanced p-AKT levels observed with Bt-NPs@SOR treatment are consistent with recent findings showing that AKT activation plays a complex role in cancer progression and treatment response (Revathidevi and Munirajan, 2019). Studies have shown that modulating multiple pathways simultaneously can potentially overcome resistance mechanisms commonly observed with single-pathway inhibition (Emran et al., 2022). This approach, combining AKT pathway modulation with other stress pathways, may create unique cellular states that enhance therapeutic efficacy (Wang et al., 2014).

The p38 MAPK pathway examination reveals striking differences in activation levels. Bt-NPs@SOR treatment resulted in the most robust p-p38/p38 ratio, significantly higher than other treatments (Fig. 7B). The strong activation of p38 MAPK by Bt-NPs@SOR is particularly significant given recent evidence linking p38 activation to enhanced therapeutic responses in HCC. Current literature suggests that sustained p38 MAPK activation can overcome resistance mechanisms and promote apoptosis in HCC cells, particularly when combined with other therapeutic stressors (Deng et al., 2024). This aligns with our observations of enhanced therapeutic efficacy despite concurrent AKT activation.

Activation of apoptotic pathway, assessed through Caspase 8 and its cleaved form (Fig. 7C), demonstrates varying levels of activation. NPs@SOR and Bt-NPs@SOR showed the highest level of cleaved caspase 8 (Kong et al., 2021). This result suggests that sorafenib delivered by nanoparticles most effectively triggers the apoptotic cascade (Sheng et al., 2017). The analysis of apoptotic signaling through caspase 8 cleavage revealed complex pathway interactions (Chen et al., 2024; Tummers and Green, 2017). Recent studies have demonstrated that effective HCC therapies often require engagement of multiple death pathways, as these tumors frequently develop resistance to single pathway targeting (Huang et al., 2020; Wu et al., 2024).

4. Conclusions

In this work, nanoparticles for sorafenib delivery have been prepared using an amphiphilic polyaminoacidic-based graft copolymer (PHEA-g-IB-pButMA-g-PEG-Bt), specifically designed for biotin-mediated active targeting of cancer cells. Nanoparticles were obtained via dialysis-based nanoprecipitation, resulting in a size suitable for both parenteral and oral administration, along with satisfactory drug loading and prolonged drug release capabilities.

The in vitro experiments demonstrated that SOR, NPs@SOR, and Bt-NPs@SOR exerted a strong antiproliferative effect on HepG2 and HuH-7 cell lines, leading to a time-dependent reduction in cell viability and progressively lower inhibitory concentrations (IC50) observed over 72 h. Notably, SOR proved highly active since the early stages (24–48 h), whereas Bt-NPs@SOR displayed a more pronounced efficacy at later time points, confirming that biotinylated polymer encapsulation enables sustained and/or enhanced tumor cell targeting. In the HuH-7 xenograft murine model, analysis of tumor samples stained with H&E and subjected to immunohistochemistry (Ki-67 and CD31) revealed potent cytotoxic and antiangiogenic activities for all treatments, with Bt-NPs@SOR associated with more extensive structural damage and a more marked decrease in proliferative index (Ki-67) and tumor vasculature (CD31). Moreover, Western blot data on proteins involved in survival (p-AKT), cellular stress and apoptotic processes (p-p38, caspase-8, cleaved caspase-8) indicate that SOR, and more prominently Bt-NPs@SOR, effectively inhibit protumor signaling pathways while promoting programmed cell death mechanisms.

Collectively, these in vitro and in vivo findings confirm that the biotinylated polymeric system (Bt-NPs@SOR) enhances sorafenib's therapeutic profile, potentially improving its clinical efficacy through prolonged and more selective drug release. These results highlight the proposed nanoparticles as promising candidates for targeted hepatocellular carcinoma therapy.

CRediT authorship contribution statement

Giulia Di Benedetto: Writing – original draft, Methodology, Investigation, Formal analysis, Data curation. **Paola Varvarà:** Writing – review & editing, Methodology, Investigation, Formal analysis, Data curation. **Salvatore Emanuele Drago:** Writing – review & editing, Methodology, Investigation, Formal analysis, Data curation. **Anna Flavia Cantone:** Writing – review & editing, Methodology, Formal analysis, Data curation. **Nicolò Mauro:** Writing – review & editing, Supervision, Methodology. **Gabriella Gaudio:** Writing – review & editing, Methodology, Formal analysis. **Chiara Burgaletto:** Writing – review & editing, Methodology, Formal analysis. **Carlo Maria Bellanca:** Writing – review & editing, Methodology, Formal analysis. **Giuseppe Broggi:** Writing – review & editing, Methodology, Formal analysis. **Rosario Caltabiano:** Writing – review & editing, Methodology, Formal analysis. **Giovanna Pitarresi:** Writing – review & editing, Supervision, Funding acquisition. **Giuseppina Cantarella:** Writing – review & editing, Supervision, Funding acquisition. **Gaetano Giammona:** Supervision, Funding acquisition, Conceptualization. **Renato Bernardini:** Writing – review & editing, Supervision, Funding acquisition.

Funding

This work was supported by POR FESR Sicilia 2014–2020 (azione 1.1.5) project: “Micro e nanosistemi innovativi per la cura efficace del Tumore al Fegato” (LiverSmartDrug) (Code project 087219090463).

Declaration of competing interest

The authors declare that they have no known competing financial interests or personal relationships that could have appeared to influence the work reported in this paper.

Acknowledgments

Authors thank ATeN Center of University of Palermo - Laboratory of Preparation and Analysis of Biomaterials, for the support in the Size Exclusion Chromatography analysis and Thermal analysis.

Paola Varvarà was supported by Fondazione Veronesi.

Appendix A. Supplementary material

Supplementary data to this article can be found online at https://doi.org/10.1016/j.ijpharm.2025.125729.

Data availability

Data will be made available on request.

References

Abdel-Rahman, O., Lamarca, A., 2017. Development of sorafenib-related side effects in patients diagnosed with advanced hepatocellular carcinoma treated with sorafenib: a systematic-review and meta-analysis of the impact on survival. Expert Rev. Gastroenterol. Hepatol. 11, 75–83. https://doi.org/10.1080/17474124.2017.1264874.

Basilio-de-Oliveira, R.P., Pannain, V.L.N., 2015. Prognostic angiogenic markers (endoglin, VEGF, CD31) and tumor cell proliferation (Ki67) for gastrointestinal stromal tumors. WJG 21, 6924–6930. https://doi.org/10.3748/wjg.v21.i22.6924.

Böttger, R., Pauli, G., Chao, P.-H., Al Fayez, N., Hohenwarter, L., Li, S.-D., 2020. Lipid-based nanoparticle technologies for liver targeting. Adv. Drug Deliv. Rev. 154–155, 79–101. https://doi.org/10.1016/j.addr.2020.06.017.

Bradford, M.M., 1976. A rapid and sensitive method for the quantitation of microgram quantities of protein utilizing the principle of protein-dye binding. Anal. Biochem. 72, 248–254. https://doi.org/10.1016/0003-2697(76)90527-3.

Bruix, J., Da Fonseca, L.G., Reig, M., 2019. Insights into the success and failure of systemic therapy for hepatocellular carcinoma. Nat. Rev. Gastroenterol. Hepatol. 16, 617–630. https://doi.org/10.1038/s41575-019-0179-x.

Cervello, M., Pitarresi, G., Volpe, A.B., Porsio, B., Balasus, D., Emma, M.R., Azzolina, A., Puleio, R., Loria, G.R., Puleo, S., Giammona, G., 2017. Nanoparticles of a polyaspartamide-based brush copolymer for modified release of sorafenib: In vitro and in vivo evaluation. J. Control. Release 266, 47–56. https://doi.org/10.1016/j.jconrel.2017.09.014.

Chen, H., Lin, Y., Chen, J., Luo, X., Kan, Y., He, Y., Zhu, R., Jin, J., Li, D., Wang, Y., Han, Z., 2024. Targeting caspase-8: a new strategy for combating hepatocellular carcinoma. Front. Immunol. 15, 1501659. https://doi.org/10.3389/fimmu.2024.1501659.

Chen, P., Kuang, W., Zheng, Z., Yang, S., Liu, Y., Su, L., Zhao, K., Liang, G., 2019. Carboxylesterase-Cleavable Biotinylated Nanoparticle for Tumor-Dual Targeted Imaging. Theranostics 9, 7359–7369. https://doi.org/10.7150/thno.37625.

Cusimano, A., Puleio, R., D'Alessandro, N., Loria, G.R., McCubrey, J.A., Montalto, G., Cervello, M., 2015. Cytotoxic activity of the novel small molecule AKT inhibitor SC66 in hepatocellular carcinoma cells. Oncotarget 6, 1707–1722. https://doi.org/10.18632/oncotarget.2738.

Daher, S., Massarwa, M., Benson, A.A., Khoury, T., 2018. Current and Future Treatment of Hepatocellular Carcinoma: An Updated Comprehensive Review. J. Clin. Transl. Hepatol. 6, 1–10. https://doi.org/10.14218/JCTH.2017.00031.

Deng, Y., Li, Y., Yang, M., Gao, Y., Luo, X., Chen, H., Guo, M., Yang, X., Liu, Y., He, J., Lu, B., Liu, N., 2024. Carfilzomib activates ER stress and JNK/p38 MAPK signaling to promote apoptosis in hepatocellular carcinoma cells. ABBS. https://doi.org/10.3724/abbs.2024040.

Emran, T.B., Shahriar, A., Mahmud, A.R., Rahman, T., Abir, M.H., Siddiquee, Mohd, F.-R., Ahmed, H., Rahman, N., Nainu, F., Wahyudin, E., Mitra, S., Dhama, K., Habiballah, M.M., Haque, S., Islam, A., Hassan, M.M., 2022. Multidrug resistance in cancer: understanding molecular mechanisms immunoprevention and therapeutic approaches. Front. Oncol. 12, 891652. https://doi.org/10.3389/fonc.2022.891652.

Finn, R., 2013. Emerging Targeted Strategies in Advanced Hepatocellular Carcinoma. Semin. Liver Dis. 33, S11–S19. https://doi.org/10.1055/s-0033-1333632.

Fu, C., Yang, R.-M., Wang, L., Li, N., Qi, M., Xu, X., Wei, X., Jiang, X.-Q., Zhang, L.-M., 2017. Surface functionalization of superparamagnetic nanoparticles by an acid-liable polysaccharide-based prodrug for combinatorial monitoring and chemotherapy of hepatocellular carcinoma. RSC Adv. 7, 41919–41928. https://doi.org/10.1039/C7RA05042A.

Giammona, G., Carlisi, B., Palazzo, S., 1987. Reaction of α,β-poly(*N* -hydroxyethyl)- DL -aspartamide with derivatives of carboxylic acids. J. Polym. Sci. A Polym. Chem. 25, 2813–2818. https://doi.org/10.1002/pola.1987.080251016.

Giammona, G., Drago, S.E., Calabrese, G., Varvarà, P., Rizzo, M.G., Mauro, N., Nicotra, G., Conoci, S., Pitarresi, G., 2022. Galactosylated Polymer/Gold Nanorods Nanocomposites for Sustained and Pulsed Chemo-Photothermal Treatments of Hepatocarcinoma. Pharmaceutics 14, 2503. https://doi.org/10.3390/pharmaceutics14112503.

Hu, J., Albadawi, H., Chong, B.W., Deipolyi, A.R., Sheth, R.A., Khademhosseini, A., Oklu, R., 2019. Advances in Biomaterials and Technologies for Vascular Embolization. Adv. Mater. 31, e1901071. https://doi.org/10.1002/adma.201901071.

Hu, X., Zhu, H., He, X., Chen, J., Xiong, L., Shen, Y., Li, J., Xu, Y., Chen, W., Liu, X., Cao, D., Xu, X., 2023. The application of nanoparticles in immunotherapy for hepatocellular carcinoma. J. Control. Release 355, 85–108. https://doi.org/10.1016/j.jconrel.2023.01.051.

Hu, Y., Du, Y., Liu, N., Liu, X., Meng, T., Cheng, B., He, J., You, J., Yuan, H., Hu, F., 2015. Selective redox-responsive drug release in tumor cells mediated by chitosan based glycolipid-like nanocarrier. J. Control. Release 206, 91–100. https://doi.org/10.1016/j.jconrel.2015.03.018.

Huang, A., Yang, X.-R., Chung, W.-Y., Dennison, A.R., Zhou, J., 2020. Targeted therapy for hepatocellular carcinoma. Sig Transduct Target Ther 5, 146. https://doi.org/10.1038/s41392-020-00264-x.

Jemal, A., Bray, F., Center, M.M., Ferlay, J., Ward, E., Forman, D., 2011. Global cancer statistics. CA Cancer J. Clin. 61, 69–90. https://doi.org/10.3322/caac.20107.

Kane, R.C., Farrell, A.T., Madabushi, R., Booth, B., Chattopadhyay, S., Sridhara, R., Justice, R., Pazdur, R., 2009. Sorafenib for the treatment of unresectable hepatocellular carcinoma. Oncologist 14, 95–100. https://doi.org/10.1634/theoncologist.2008-0185.

Kong, F.-H., Ye, Q.-F., Miao, X.-Y., Liu, X., Huang, S.-Q., Xiong, L., Wen, Y., Zhang, Z.-J., 2021. Current status of sorafenib nanoparticle delivery systems in the treatment of hepatocellular carcinoma. Theranostics 11, 5464–5490. https://doi.org/10.7150/thno.54822.

Landesman-Milo, D., Peer, D., 2016. Transforming nanomedicines from lab scale production to novel clinical modality. Bioconjug. Chem. 27, 855–862. https://doi.org/10.1021/acs.bioconjchem.5b00607.

Liu, Y., Li, J., Liu, F., Zhang, L., Feng, L., Yu, D., Zhang, N., 2015. Theranostic Polymeric Micelles for the Diagnosis and Treatment of Hepatocellular Carcinoma. J. Biomed. Nanotechnol. 11, 613–622. https://doi.org/10.1166/jbn.2015.1945.

Llovet, J.M., Kelley, R.K., Villanueva, A., Singal, A.G., Pikarsky, E., Roayaie, S., Lencioni, R., Koike, K., Zucman-Rossi, J., Finn, R.S., 2021. Hepatocellular Carcinoma. Nat. Rev. Dis. Primers 7, 6. https://doi.org/10.1038/s41572-020-00240-3.

Llovet, J.M., Pinyol, R., Kelley, R.K., El-Khoueiry, A., Reeves, H.L., Wang, X.W., Gores, G.J., Villanueva, A., 2022. Molecular pathogenesis and systemic therapies for hepatocellular carcinoma. Nat Cancer 3, 386–401. https://doi.org/10.1038/s43018-022-00357-2.

Llovet, J.M., Ricci, S., Mazzaferro, V., Hilgard, P., Gane, E., Blanc, J.-F., De Oliveira, A.C., Santoro, A., Raoul, J.-L., Forner, A., Schwartz, M., Porta, C., Zeuzem, S., Bolondi, L., Greten, T.F., Galle, P.R., Seitz, J.-F., Borbath, I., Häussinger, D., Giannaris, T., Shan, M., Moscovici, M., Voliotis, D., Bruix, J., 2008. Sorafenib in Advanced Hepatocellular Carcinoma. N. Engl. J. Med. 359, 378–390. https://doi.org/10.1056/NEJMoa0708857.

Ma, Y., Xu, R., Liu, X., Zhang, Y., Song, L., Cai, S., Zhou, S., Xie, Y., Li, A., Cao, W., Tang, X., 2021. LY3214996 relieves acquired resistance to sorafenib in hepatocellular carcinoma cells. Int. J. Med. Sci. 18, 1456–1464. https://doi.org/10.7150/ijms.51256.

Mauro, N., Utzeri, M.A., Cillari, R., Scialabba, C., Giammona, G., Cavallaro, G., 2022. Cholesterol-Inulin Conjugates for Efficient SN38 Nuclear Delivery: Nanomedicines for Precision Cancer Therapy. Cancers 14, 4857. https://doi.org/10.3390/cancers14194857.

Metkar, S.P., Fernandes, G., Navti, P.D., Nikam, A.N., Kudarha, R., Dhas, N., Seetharam, R.N., Santhosh, K.V., Rao, B.S.S., Mutalik, S., 2023. Nanoparticle drug delivery systems in hepatocellular carcinoma: A focus on targeting strategies and therapeutic applications. OpenNano 12, 100159. https://doi.org/10.1016/j.onano.2023.100159.

Revathidevi, S., Munirajan, A.K., 2019. Akt in cancer: Mediator and more. Semin. Cancer Biol. 59, 80–91. https://doi.org/10.1016/j.semcancer.2019.06.002.

Romualdo, G.R., Leroy, K., Costa, C.J.S., Prata, G.B., Vanderborght, B., Da Silva, T.C., Barbisan, L.F., Andraus, W., Devisscher, L., Câmara, N.O.S., Vinken, M., Cogliati, B., 2021. In Vivo and In Vitro Models of Hepatocellular Carcinoma: Current Strategies for Translational Modeling. Cancers 13, 5583. https://doi.org/10.3390/cancers13215583.

Scarabel, L., Perrone, F., Garziera, M., Farra, R., Grassi, M., Musiani, F., Russo Spena, C., Salis, B., De Stefano, L., Toffoli, G., Rizzolio, F., Tonon, F., Abrami, M., Chiarappa, G., Pozzato, G., Forte, G., Grassi, G., Dapas, B., 2017. Strategies to optimize siRNA delivery to hepatocellular carcinoma cells. Expert Opin. Drug Deliv. 14, 797–810. https://doi.org/10.1080/17425247.2017.1292247.

Seidu, T.A., Kutoka, P.T., Asante, D.O., Farooq, M.A., Alolga, R.N., Bo, W., 2022. Functionalization of Nanoparticulate Drug Delivery Systems and Its Influence in Cancer Therapy. Pharmaceutics 14, 1113. https://doi.org/10.3390/pharmaceutics14051113.

Sheng, X., Huang, T., Qin, J., Li, Q., Wang, W., Deng, L., Dong, A., 2017. Preparation, pharmacokinetics, tissue distribution and antitumor effect of sorafenib-incorporating nanoparticles in vivo. Oncol. Lett. 14, 6163–6169. https://doi.org/10.3892/ol.2017.6934.

Singh, A., Mishra, S., Sharma, S., Ojha, S., Yagnik, S., Pandey, S., 2023. Ligand-mediated Targeted Drug Delivery Approaches against HepatocellularCarcinoma. CCDT 23, 879–888. https://doi.org/10.2174/1568009623666230503094346.

Song, S.-S., Xia, B.-Y., Chen, J., Yang, J., Shen, X., Fan, S.-J., Guo, M., Sun, Y.-M., Zhang, X.-D., 2014. Two dimensional TiO_2 nanosheets: in vivo toxicity investigation. RSC Adv. 4, 42598–42603. https://doi.org/10.1039/C4RA05953K.

Tummers, B., Green, D.R., 2017. Caspase-8: regulating life and death. Immunol. Rev. 277, 76–89. https://doi.org/10.1111/imr.12541.

Varghese, F., Bukhari, A.B., Malhotra, R., De, A., 2014. IHC Profiler: An Open Source Plugin for the Quantitative Evaluation and Automated Scoring of Immunohistochemistry Images of Human Tissue Samples. PLoS One 9, e96801. https://doi.org/10.1371/journal.pone.0096801.

Varvarà, P., Emanuele Drago, S., Esposito, E., Campolo, M., Mauro, N., Calabrese, G., Conoci, S., Morganti, D., Fazio, B., Giammona, G., Pitarresi, G., 2024. Biotinylated polyaminoacid-based nanoparticles for the targeted delivery of lenvatinib towards hepatocarcinoma. Int. J. Pharm. 662, 124537. https://doi.org/10.1016/j.ijpharm.2024.124537.

Wang, C., Xiu, Y., Zhang, Y., Wang, Y., Xu, J., Yu, W., Xing, D., 2025. Recent advances in biotin-based therapeutic agents for cancer therapy. Nanoscale 17, 1812–1873. https://doi.org/10.1039/D4NR03729D.

Wang, H., Xu, L., Zhu, X., Wang, P., Chi, H., Meng, Z., 2014. Activation of phosphatidylinositol 3-kinase/Akt signaling mediates sorafenib-induced invasion and metastasis in hepatocellular carcinoma. Oncol. Rep. 32, 1465–1472. https://doi.org/10.3892/or.2014.3352.

Wang, Y.-Q., Huang, C., Ye, P.-J., Long, J.-R., Xu, C.-H., Liu, Y., Ling, X.-L., Lv, S.-Y., He, D.-X., Wei, H., Yu, C.-Y., 2022. Prolonged blood circulation outperforms active targeting for nanocarriers-mediated enhanced hepatocellular carcinoma therapy in vivo. J. Control. Release 347, 400–413. https://doi.org/10.1016/j.jconrel.2022.05.024.

Wilhelm, S., Tavares, A.J., Dai, Q., Ohta, S., Audet, J., Dvorak, H.F., Chan, W.C.W., 2016. Analysis of nanoparticle delivery to tumours. Nat. Rev. Mater. 1, 16014. https://doi.org/10.1038/natrevmats.2016.14.

Wu, X., Cao, J., Wan, X., Du, S., 2024. Programmed cell death in hepatocellular carcinoma: mechanisms and therapeutic prospects. Cell Death Discov. 10, 356. https://doi.org/10.1038/s41420-024-02116-x.

Yang, X., Xia, W., Chen, L., Wu, C.X., Zhang, C.C., Olson, P., Wang, X.Q., 2018. Synergistic antitumor effect of a γ-secretase inhibitor PF-03084014 and sorafenib in hepatocellular carcinoma. Oncotarget 9, 34996–35007. https://doi.org/10.18632/oncotarget.26209.

Yu, Z., Huang, L., Guo, J., 2024. Anti-stromal nanotherapeutics for hepatocellular carcinoma. J. Controll. Release 367, 500–514. https://doi.org/10.1016/j.jconrel.2024.01.050.

Yuan, F., Dellian, M., Fukumura, D., Leunig, M., Berk, D.A., Torchilin, V.P., Jain, R.K., 1995. Vascular permeability in a human tumor xenograft: molecular size dependence and cutoff size. Cancer Res. 55, 3752–3756.

Zhang, G., Wang, Y., Fuchs, B.C., Guo, W., Drum, D.L., Erstad, D.J., Shi, B., DeLeo, A.B., Zheng, H., Cai, L., Zhang, L., Tanabe, K.K., Wang, X., 2022. Improving the therapeutic efficacy of sorafenib for hepatocellular carcinoma by repurposing disulfiram. Front. Oncol. 12, 913736. https://doi.org/10.3389/fonc.2022.913736.